NeuroImage 185 (2019) 154–163

Contents lists available at ScienceDirect

NeuroImage

journal homepage: www.elsevier.com/locate/neuroimage

Cerebral blood volume changes during the BOLD post-stimulus undershoot measured with a combined normoxia/hyperoxia method

Eulanca Y. Liu [a,b], Frank Haist [c,d], David J. Dubowitz [b,e], Richard B. Buxton [b,e,*]

[a] Neurosciences Graduate Program, Medical Scientist Training Program, University of California, San Diego, USA
[b] Center for Functional MRI, University of California, San Diego, USA
[c] Psychiatry, University of California, San Diego, USA
[d] Center for Human Development, University of California, San Diego, USA
[e] Radiology, University of California, San Diego, USA

ARTICLE INFO

Keywords:
Functional MRI
Blood oxygenation level dependent
Cerebral blood volume
Hyperoxia
Post-stimulus undershoot
Cerebral metabolism of oxygen

ABSTRACT

Cerebral blood flow (CBF) and blood oxygenation level dependent (BOLD) signal measurements make it possible to estimate steady-state changes in the cerebral metabolic rate of oxygen ($CMRO_2$) with a calibrated BOLD method. However, extending this approach to measure the dynamics of $CMRO_2$ requires an additional assumption: that deoxygenated cerebral blood volume (CBV_{dHb}) follows CBF in a predictable way. A test-case for this assumption is the BOLD post-stimulus undershoot, for which one proposed explanation is a strong uncoupling of flow and blood volume with an elevated level of CBV_{dHb} during the post-stimulus period compared to baseline due to slow blood volume recovery (Balloon Model). A challenge in testing this model is that CBV_{dHb} differs from total blood volume, which can be measured with other techniques. In this study, the basic hypothesis of elevated CBV_{dHb} during the undershoot was tested, based on the idea that the BOLD signal change when a subject switches from breathing a normoxic gas to breathing a hyperoxic gas is proportional to the absolute CBV_{dHb}. In 19 subjects (8F), dual-echo BOLD responses were measured in primary visual cortex during a flickering radial checkerboard stimulus in normoxia, and the identical experiment was repeated in hyperoxia (50% O_2/balance N_2). The BOLD signal differences between normoxia and hyperoxia for the pre-stimulus baseline, stimulus, and post-stimulus periods were compared using an equivalent BOLD signal calculated from measured R_2* changes to eliminate signal drifts. Relative to the pre-stimulus baseline, the average BOLD signal change from normoxia to hyperoxia was negative during the undershoot period ($p = 0.0251$), consistent with a reduction of CBV_{dHb} and contrary to the prediction of the Balloon Model. Based on these results, the BOLD post-stimulus undershoot does not represent a case of strong uncoupling of CBV_{dHb} and CBF, supporting the extension of current calibrated BOLD methods to estimate the dynamics of $CMRO_2$.

1. Introduction

Functional magnetic resonance imaging (fMRI) based on measurement of the blood-oxygenation level dependent (BOLD) signal is widely used for mapping patterns of activation in the human brain. However, interpretation of the BOLD response in terms of the underlying physiological changes is challenging due to the complexity of the signal. The BOLD signal is primarily due to a change in total deoxyhemoglobin (Buxton, 2013), determined by changes in cerebral blood flow (CBF), cerebral metabolic rate of oxygen ($CMRO_2$), and cerebral blood volume (CBV).

Although the physiological ambiguity of the BOLD signal is a major challenge for interpreting BOLD data alone, it offers the potential for a deeper probe of the physiology when combined with an additional independent measurement of CBF using an arterial spin labeling (ASL) method. The CBF and BOLD measurements, combined with an appropriate calibration measurement, make it possible to estimate $CMRO_2$ changes (Davis et al., 1998). Measurements of $CMRO_2$ are challenging with any methodology, and this calibrated BOLD approach is now a leading tool for probing oxygen metabolism in the human brain (Pike, 2012). However, a confounding effect for measuring $CMRO_2$ changes is a

Abbreviations: CBV_{dHb}, Deoxygenated cerebral blood volume; ASL, Arterial spin labeling; PICORE, Proximal inversion with control of off-resonance effects; QUIPSS II, Quantitative imaging of perfusion using a single subtraction II.

* Corresponding author. University of California, San Diego, 9500 Gilman Drive, MC 0677, La Jolla, CA, 92093-0677, USA.
E-mail address: rbuxton@ucsd.edu (R.B. Buxton).

https://doi.org/10.1016/j.neuroimage.2018.10.032
Received 21 February 2018; Received in revised form 9 October 2018; Accepted 9 October 2018
Available online 10 October 2018
1053-8119/

change in CBV, which also affects the BOLD signal. Typically, calibrated BOLD studies measure changes between two steady-states, with the assumption that the CBV can be assumed to follow CBF in a steady-state relationship based on previous measurements; this is usually modeled as a power law relationship (Grubb et al., 1974). Extending the calibrated BOLD approach to measure the dynamics of $CMRO_2$ involves a key question: does CBV dynamically follow CBF, so that the dynamics of CBV can be taken into account in the analysis?

The BOLD post-stimulus undershoot has been a prime example of the ambiguity of separating $CMRO_2$ and CBV effects in the BOLD response. The undershoot is a reduction, relative to the baseline, of the BOLD signal after the end of the stimulus that may persist for tens of seconds before the signal returns to baseline. The phenomenon has been observed since the beginning of fMRI (Kwong et al., 1992), and yet there is still no consensus in the field on the physiological origin of the undershoot (van Zijl et al., 2012). Possible interpretations include a slow recovery of CBV (Buxton et al., 1998; Mandeville et al., 1999), a slow recovery of $CMRO_2$ (Frahm et al., 2008; van Zijl et al., 2012), or a CBF undershoot (Chen and Pike, 2009a,b). For extending calibrated BOLD methods to measuring the dynamics of $CMRO_2$, two of these possibilities are not a problem because different dynamics of CBF and $CMRO_2$ could potentially be untangled with simultaneous measurements of CBF and BOLD dynamics. The problem is the first hypothesis, an uncoupling of CBV and CBF, with CBV recovering to baseline more slowly than CBF and $CMRO_2$. The BOLD post-stimulus undershoot thus presents an important test case: if the undershoot is due to a mechanism such as delayed CBV recovery—an extended transient uncoupling of CBF and CBV—then dynamic measurements of $CMRO_2$ are problematic.

Experimentally testing for a transient uncoupling of CBF and CBV has its own challenges; specifically, exactly what is meant by blood volume? The BOLD response is determined by how deoxyhemoglobin (dHb) leads to relaxation of the net signal. The relevant blood volume is a dHb-weighted average over all vascular volumes (CBV_{dHb}), dominated by venous vessels, but also including capillaries and some contribution from partially deoxygenated arterioles. In simple models of the BOLD effect, CBV_{dHb} is often taken as the venous blood volume, where the blood is most deoxygenated, but other blood compartments also contribute. Averaging over blood compartments is further complicated by the effects of diffusion near the smallest vessels, where a given amount of deoxyhemoglobin in a capillary will have less of an effect on relaxation than it would if it were in a larger vein (Buxton, 2013). For this reason, the correspondence between CBV_{dHb} and standard anatomical vascular compartments is somewhat complicated. Measurements of total CBV may be a poor reflection of CBV_{dHb}, and while measurements of venous CBV should capture the dominant contribution to CBV_{dHb}, some contributions will be missed. Nevertheless, most of our current understanding of CBV dynamics is based on measurements of anatomical vascular compartments (Buxton et al., 1998; Drew et al., 2011; Kim and Kim, 2011; Mandeville et al., 1998).

Here, we report results using a promising approach for a more definitive test of CBV_{dHb} dynamics based on the effects of hyperoxia (Blockley et al., 2013, 2012). This approach exploits the idea that increasing the arterial pO_2 leads to a decrease in the tissue relaxation rate R_2*—a hyperoxia-BOLD effect—that is proportional to the deoxygenated blood volume. In the context of a detailed framework for the BOLD response developed by Griffeth et al. (Griffeth and Buxton, 2011), a new interpretation of the R_2* change with hyperoxia as a direct reflection of CBV_{dHb} was developed by Blockley and colleagues (Blockley et al., 2015, 2013, 2012). The essential idea is that the added arterial concentration of O_2 as dissolved gas diffuses quickly into tissue, offsetting the amount of oxygen needed to be removed from hemoglobin. This raises hemoglobin saturation in all blood compartments that contain deoxyhemoglobin in the normoxic state. This change in saturation, however, only weakly depends on resting OEF or hematocrit (Blockley et al., 2013). The R_2* difference for a particular state in hyperoxia versus normoxia is then directly proportional to CBV_{dHb}, with a proportionality constant that depends on the global change in arterial pO_2 (Blockley et al., 2013). The hyperoxia approach offers a way to test CBV_{dHb} dynamics by measuring the response to a stimulus in both normoxia and hyperoxia, and comparing the BOLD signal difference between hyperoxia and normoxia at different time points in the response.

We measured responses to a visual stimulus in both normoxia and hyperoxia and calculated the hyperoxia-BOLD effect, the change in R_2* (ΔR_2*) between hyperoxia and normoxia ($\Delta R_2^* = R_2^*{}_{hyperoxia} - R_2^*{}_{normoxia}$), at each time point in the baseline, stimulus, and post-stimulus periods. Ideally, ΔR_2* should be proportional to absolute CBV_{dHb} at each time point. However, other confounding factors associated with hyperoxia, such as additional changes in R_2* related to gas delivery or physiological changes in CBF and $CMRO_2$, may lead to an overall shift of R_2* between normoxia and hyperoxia. To minimize such effects, we focused on the difference between ΔR_2* during the undershoot (or during the stimulus) and ΔR_2* for the baseline state, reflecting the absolute volume change ΔCBV_{dHb} from baseline. The prediction of the Balloon Model is that CBV_{dHb} is elevated compared to baseline during the undershoot, which in turn predicts that ΔR_2* should be larger in the undershoot state than the baseline state. Our primary finding was the opposite pattern, arguing against an elevated blood volume. However, the cost of dealing with a measurement sensitive to CBV_{dHb} rather than anatomical vascular compartments is that the signal changes are small, and hyperoxia may produce additional effects that could alter the measurements. To aid in the interpretation of this result we also include modeling to define the predicted measurements and explore different potential confounding effects.

2. Methods

The primary experiment involved measuring stimulus responses under conditions of hyperoxia and normoxia. In addition, the study included a hypercapnia measurement as part of the protocol to perform a calibrated BOLD experiment (Davis et al., 1998) needed for the modeling aspects of the study.

2.1. Subjects

Twenty-one healthy adults were recruited for the study. Two subjects were eliminated from the analyses because inspired and end-tidal O_2 and CO_2 measurements revealed leaks in the tubing or non-rebreathing facemask. Thus, the study sample included 19 subjects (8 female, mean age = 24.9 years, range 20–31 years). The study was approved by the Human Research Protections Program of the University of California, San Diego; written informed consent was obtained from all subjects. Subjects were remunerated for their participation.

2.2. Gas administration

Inspired and end-tidal O_2 and CO_2 were monitored for all subjects throughout the run using a Perkin Elmer 1100 medical gas spectrometer (Perkin Elmer, Waltham, MA). Subjects were equipped with a non-rebreathing facemask (Hans Rudolph, KS, USA). The inspiratory port of the mask was connected to large gas-tight balloons (VacuMed, CA, USA), pre-filled with the appropriate gas mixtures. Gas mixtures were purchased pre-mixed (Airgas-West, CA, USA); the hyperoxic condition utilized 50% O_2, balance N_2, while hypercapnia was 5% CO_2, 21% O_2, balance N_2. The tubing (VacuMed, CA, USA) was disconnected to allow the subject to breathe normal room air in the normoxic condition.

2.3. Imaging

A dual-echo spiral PICORE QUIPSS II ASL acquisition (Wong et al., 1998) was used to acquire simultaneous BOLD and ASL dynamic images on a General Electric (GE) Discovery MR750 3.0T scanner. The acquisition prescription consisted of 7 axial slices (5 mm thick/1 mm gap)

covering the occipital cortex, centered around the calcarine sulcus, with TR = 2500 ms, TI1 = 700 ms, TI2 = 1750 ms, TE = 3.3/30 ms, 90° flip angle, FOV 256 mm, and matrix 64 × 64. A field map was acquired using the same slice prescription to correct distortions in the spiral acquisition due to magnetic field inhomogeneity (Noll et al., 2005). Physiological monitoring was performed throughout the scan session using a pulse oximeter for cardiac cycle monitoring and respiratory bellows for respiratory dynamics (GE MR750 built-in). A cerebral spinal fluid (CSF) reference was obtained for CBF quantification (Chalela et al., 2000; Liu et al., 2004; Perthen et al., 2008) using a single-shot EPI acquisition (TE = 3.3 ms, TR = 4000 ms); a minimum contrast scan (eight-shot spiral acquisition, TE = 11 ms, TR = 2000 ms) was acquired to map and correct for transmit and receiver coil inhomogeneities (Wang et al., 2005). These latter acquisitions used the same prescription as the ASL acquisition. A high resolution T_1-weighted anatomical scan (FSPGR) was acquired for each subject for image registration.

2.4. Stimulus paradigm

The task used to elicit neural activity in the occipital lobe (V1) was a black and white flickering radial checkerboard presented using MATLAB (2014a, The MathWorks, MA, USA) with the Psychophysics Toolbox extensions (Brainard, 1997; Pelli, 1997). The checkerboard contrast and luminance were as described in previous work (Simon et al., 2016); the central region, with visual angle ~1.5°, was maintained at iso-luminant gray, with 6 Hz light-dark reversal frequency. The subject could view the stimulus, projected onto a screen, through a mirror set atop the head coil.

The study consisted of an 18-min run during which both BOLD and CBF-weighted images were acquired. The run was composed of a 3-min functional localizer, a normoxia/normocapnia (room air) block, a hypercapnia block, and a hyperoxia block. See Fig. 1A for a representation of the run design. Throughout the run, subjects fixated on a cross projected in the center of the screen, on top of which single digit numbers were superimposed for a 1-back task. Subjects performed the task (Kirchner, 1958) continuously throughout the run. The 1-back task consisted of random single digit numbers displayed at 1-sec intervals; subjects were instructed to press a button on a response box each time they observed the same digit displayed sequentially. The 1-back task was used solely to help the subjects maintain fixation and wakefulness, and was not treated as an activation task in any of the analyses. The 3-min functional localizer consisted of three 30-sec ON/30-sec OFF blocks of the visual stimulus to strongly activate the visual cortex. Following the localizer and a 1-min baseline, the 4-min normoxia block was presented that consisted of two 1-min ON/1-min OFF blocks of the visual stimulus while the subject breathed room air. Next, a 3-min hypercapnia challenge was conducted, with the subject breathing the hypercapnia mixture in the baseline state. After hypercapnia administration, subjects were switched to breathing the hyperoxia mixture. Two minutes were allowed for gas equilibration. The final segment was a 1-min baseline and 4 min of 1-min ON/1-min OFF blocks of the visual stimulus in hyperoxia.

2.5. Data analysis

2.5.1. Constructing separate CBF and BOLD images

Raw ASL images were first distortion corrected using the field map acquisition to account for inhomogeneity in the magnetic field (Noll et al., 2005). The time series data were motion corrected and registered to one image in the 18-min run using AFNI software (Cox, 1996). The first four images of the run were discarded to allow the signal to reach steady state. Minimum contrast images were used to correct ASL data for coil sensitivity inhomogeneity (Wang et al., 2005). Applying surround-subtraction to the raw first-echo ASL images produced CBF-weighted images with minimal contamination from BOLD (Liu and Wong, 2005). BOLD-weighted images were constructed for both echoes with a surround average of the ASL time series, designed to minimize CBF-weighting (Liu and Wong, 2005).

2.5.2. Region of interest (ROI) responses

ROIs were generated using the CBF-weighted images and the second echo BOLD responses to the 3-min functional localizer. A general linear model approach, described by Perthen et al. (2008), was used for ROI selection. The pattern of the stimulus was convolved with a gamma density function to produce a stimulus regressor (Boynton et al., 1996). A constant and a linear term were used as nuisance regressors. A gray matter mask was generated from the average CBF with a cut-off of 2 times the mean of the average CBF across all slices. ROI selection was also restricted to the posterior third of the brain. Voxels exhibiting both CBF and BOLD were selected using an overall significance threshold of $p = 0.05$ and minimum cluster size of 4. In this way, an active visual ROI defined solely from voxels activated by the functional localizer was identified for each subject based on exhibiting both CBF and BOLD activation independently. ROI-averaged CBF-weighted and first and second echo BOLD-weighted time series were generated for each subject. Due to the long duration of the run, we removed a linear baseline from the data calculated as a fit to the baseline periods, defined as the mean of the 15 s of rest before the first normoxia visual stimulus (at the 4-min mark), the 15 s of rest before the second normoxia visual stimulus (at the 6-min mark), and the 15 s of rest before the CO_2 stimulus onset (at the 8-min mark). Each time series was normalized to the average baseline value after the correction for linear drift. These normalized values were

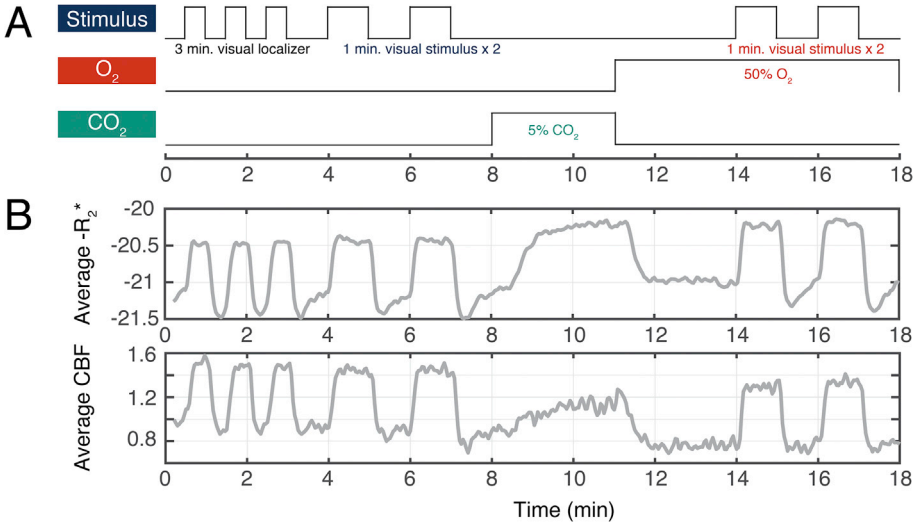

Fig. 1. Experimental design and raw data. (A) Schematic of normoxic, hyperoxic, and calibrated BOLD hypercapnic gas experiments with visual stimuli (a 6 Hz flickering checkerboard was presented in 1-min ON blocks repeated twice, with 1-min OFF blocks between) and functional localizer. CBF and BOLD responses were acquired simultaneously with PICORE QUIPSS II (Wong et al., 1998) (TR = 2500 ms, TI1 = 700 ms, TI2 = 1750 ms, TE = 3.3/30 ms). (B) Top: Average BOLD response (19 subjects) expressed as $-R_2^*$ over the entire 18-min sequence. Bottom: Average CBF response over entire 18-min sequence. CBF values have been adjusted to correct for decreased T_1 of blood due to hyperoxia beginning at the 11-min mark (Bulte et al., 2007).

used for all subsequent analyses. For the CBF data, we expected there to be an artifactual lowering of the ASL signal due to the T_1 shortening effect of hyperoxia. Based on the work of Bulte and colleagues (Bulte et al., 2007), we took estimates of the T_1 of blood as 1.66 s for air and 1.50 s for the $FiO_2 = 0.5$ of our experiment. In our pulsed ASL method we expect the ASL signal to be attenuated approximately by an exponential in $TI2/T_1$ (Wong et al., 1998), giving an estimated correction factor of 1.12 between breathing air and breathing the hyperoxic mixture. The apparent CBF values were multiplied by this factor beginning with data points at the 11-min mark, when hyperoxia was administered.

2.5.3. Quantitative R_2* measurements

For the ROI, a time series of R_2* was calculated from the first and second echo BOLD time series as: $R_2^*(t) = ln\left(\frac{S(TE1)}{S(TE2)}\right) \Big/ (TE2 - TE1)$, where S(TE1) and S(TE2) are the signals at the first and second echoes at time t during the run. One advantage of working with R_2* is that it removes systematic effects of drift that scale both echo intensities in the same way. The average value over the defined baseline periods was calculated and subtracted to form a time series δR_2*(t). For some of the subsequent analyses we converted δR_2*(t) back to an equivalent "cleaned" BOLD signal without the drift effects as: $\delta b(t) = 1 - exp[-TE2 \cdot \delta R_2^*(t)]$.

2.5.4. Hyperoxia-BOLD response ($\Delta BOLD_{h\text{-}n}$)

Here we define the hyperoxia-BOLD response for a given state $\Delta R_2{*}_{h\text{-}n}$ as the difference between δR_2* measured during hyperoxia and δR_2* measured during normoxia. These values $\Delta R_2{*}_{h\text{-}n}$ were converted to equivalent hyperoxia-BOLD responses ($\Delta BOLD_{h\text{-}n}$). For each gas condition the two visual stimulus blocks were averaged. The resulting data are a 2.5-min time course consisting of a 30-sec baseline, 1-min visual stimulus, and 1-min undershoot period and return to baseline. We focused on the average change for three states: Baseline, defined as the mean of the 30-sec window before onset of the visual stimulus and the last 15 s of the 1-min rest window after stimulus termination; Activation, defined as the last 30 s of the stimulus block; and Undershoot, defined as starting 10 s after the end of the stimulus and continuing for 30 s. For each period, the average $\Delta BOLD_{h\text{-}n}$ was calculated. Based on the modeling of the effects of hyperoxia (Blockley et al., 2013), for the ideal experiment each of these $\Delta BOLD_{h\text{-}n}$ values should be proportional to the absolute CBV_{dHb} in that state. In practice, we expect that additional effects of administering hyperoxia may lead to an additional shift of R_2* (Pilkinton et al., 2011). To minimize this effect we focused on the difference of $\Delta BOLD_{h\text{-}n}$ values between the baseline and the activation and undershoot states.

2.5.5. CO_2 responses

For each subject the ROI-averaged BOLD and CBF responses to hypercapnia were calculated from the mean of the baseline period, taken as the 30-sec window prior to administration of CO_2, and from the mean of the CO_2 period, taken as the 2-min window at the end of the CO_2 inhalation block (one minute after onset of CO_2 administration).

3. Results

3.1. Experimental results

Subject inhalation of the hyperoxic gas mixture produced a measured difference in end-tidal pO_2 of $+189 \pm 15$ mmHg compared to normoxia. The average CBF and R_2* time courses are shown in Fig. 1. In the baseline state the mean R_2* in the selected ROI was 21.2 ± 0.04 s^{-1}, and decreased by 0.13 ± 0.1 s^{-1} following inhalation of the hyperoxic gas. The mean dynamic R_2* curve across subjects is plotted in the top panel of Fig. 1B, presented as the negative of R_2* ($-R_2$*) to visually resemble the BOLD response.

The mean ASL signal in the baseline state decreased by approximately 22% between normoxia and hyperoxia. This decrease is likely to be due to a combination of a reduction of the T_1 of blood due to the added O_2 and a reduction of CBF associated with the hyperoxia experiment. After the estimated correction for T_1 changes was applied, the CBF was still reduced in hyperoxia compared with baseline by 13% ±5%. There was a significant difference ($p = 0.0009$) between the end-tidal CO_2 levels of the hyperoxia and normoxia conditions. The reduction (3.6%) could be causing the reduced CBF during hyperoxia since decreased CO_2 causes vasoconstriction.

After converting the R_2* measurements to a clean BOLD signal, the average data for the activation responses in normoxic and hyperoxic states, and the responses to hypercapnia data, are shown in Fig. 2 as averages across the subjects. Plotted in Fig. 2A are the fractional changes in CBF and BOLD signal (δCBF and δBOLD) from the baseline state during the activation and undershoot periods in each of the normoxic and

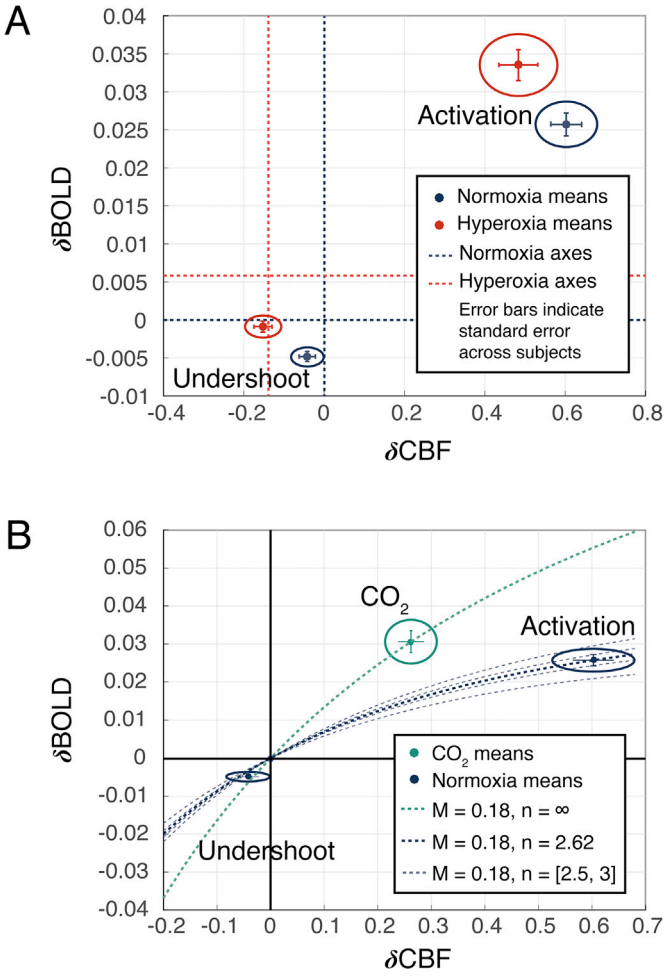

Fig. 2. CBF and BOLD changes. (A) Mean fractional BOLD and CBF (δBOLD, δCBF) changes in activation and undershoot periods during normoxia and hyperoxia (19 subjects). Error bars reflect standard deviation. Separate axes are depicted for the normoxia (blue dashed lines) and hyperoxia (red dashed lines) experiments to demonstrate the shift in baseline BOLD and CBF with the application of hyperoxia. The data points for average activation and undershoot levels are then plotted on the corresponding gas state's axes, as indicated by matching color. Ellipses show 95% confidence interval around means. (B) Teal data point represents flow and BOLD change in the hypercapnia experiment. Ellipses around each data point indicate 95% confidence interval. Dashed lines indicate regions of similar relationship between BOLD and CBF, and thus CBF and $CMRO_2$ coupling ($n = CMRO_2/CBF$), given the possible range of error and $M = 0.18$ (calculated from BOLD/CBF measurements during 5% CO_2 calibration), $\alpha = 0.2$, and $\beta = 1$.

hyperoxic gas conditions. In Fig. 2A, the shifted axes for the hyperoxia plot (red dashed lines) indicates the change in CBF and BOLD induced purely by administering hyperoxia. Baseline shifts for CBF and BOLD from normoxia to hyperoxia were −0.13 and 0.0059, respectively, expressed as a fractional change from their respective baselines in normoxia (blue dashed lines). Fractional δCBF and δBOLD were calculated from the respective gas-state baselines to the stimulus state (activation or undershoot). Table 1 summarizes these fractional changes in each gas state and the measured CO_2 responses. Fig. 2B plots the average measured CO_2 responses with the normoxic responses only (both activation and undershoot) for comparison, with reference lines showing various $CMRO_2$ and CBF coupling ratios ($n = CMRO_2/CBF$).

Dynamics of BOLD and CBF responses in normoxia and hyperoxia are illustrated in Fig. 3. BOLD changes to the visual stimulus (Fig. 3B, Table 1) clearly depict a significant undershoot after the stimulus ends in both hyperoxia and normoxia. The hyperoxia-BOLD effect, the difference between R_2* in the hyperoxic and normoxic conditions, is shown in (Fig. 3C). The change $\Delta BOLD_{h\text{-}n}$ is significantly negative (Table 1) in the undershoot window ($p = 0.0251$), and in the activation period there was a strong trend for a positive value that did not reach statistical significance ($p = 0.0509$). We also tested these data in a different way, motivated by the idea that the Balloon Model predicts that the difference between the activation value and the undershoot value should be smaller than the difference between the activation value and the baseline value, corresponding to elevated CBV_{dHb} during the undershoot. Calculating this difference on an individual subject basis, the activation/undershoot difference was significantly larger than the activation/baseline difference ($p < 0.00001$).

The CBF in normoxia showed a modest but statistically significant undershoot from baseline ($p = 0.041$, Fig. 3A, Table 1). There was no significant CBF undershoot in the hyperoxia data ($p = 0.221$).

3.2. Modeling results

To aid with the interpretation of the data, we modeled the BOLD signal change to estimate the predicted experimental effects under different scenarios, working with the average experimental responses described above. Our primary goal was to address the basic hypothesis of the Balloon Model: is the deoxyhemoglobin (dHb)-weighted blood volume elevated above baseline in the BOLD post-stimulus undershoot period?

Table 1
Summary of average CBF and BOLD values in visual activation window, undershoot window, and CO_2 administration window. P-values are representative of difference from zero.

BOLD changes			
	Fractional change	Standard error	P-value
Activation			
$BOLD_{normoxia}$	+0.0257	0.002	<0.00001
$BOLD_{hyperoxia}$	+0.0276	0.002	<0.00001
$\Delta BOLD_{h\text{-}n}$	+0.002	0.001	0.0509
Undershoot			
$BOLD_{normoxia}$	- 0.0049	0.0006	<0.00001
$BOLD_{hyperoxia}$	- 0.0068	0.0007	<0.00001
$\Delta BOLD_{h\text{-}n}$	- 0.002	0.0008	0.0251
CO_2			
$BOLD_{CO2}$	+0.0306	0.003	<0.00001
CBF changes			
	Fractional change	Standard error	P-value
Activation			
$CBF_{normoxia}$	+0.603	0.038	<0.00001
$CBF_{hyperoxia}$	+0.608	0.048	<0.00001
$\Delta CBF_{h\text{-}n}$	+0.005	0.002	0.883
Undershoot			
$CBF_{normoxia}$	- 0.0421	0.020	0.0414
$CBF_{hyperoxia}$	- 0.0278	0.023	0.221
$\Delta CBF_{h\text{-}n}$	+0.0143	0.0006	0.658
CO_2			
CBF_{CO2}	+0.262	0.024	<0.00001

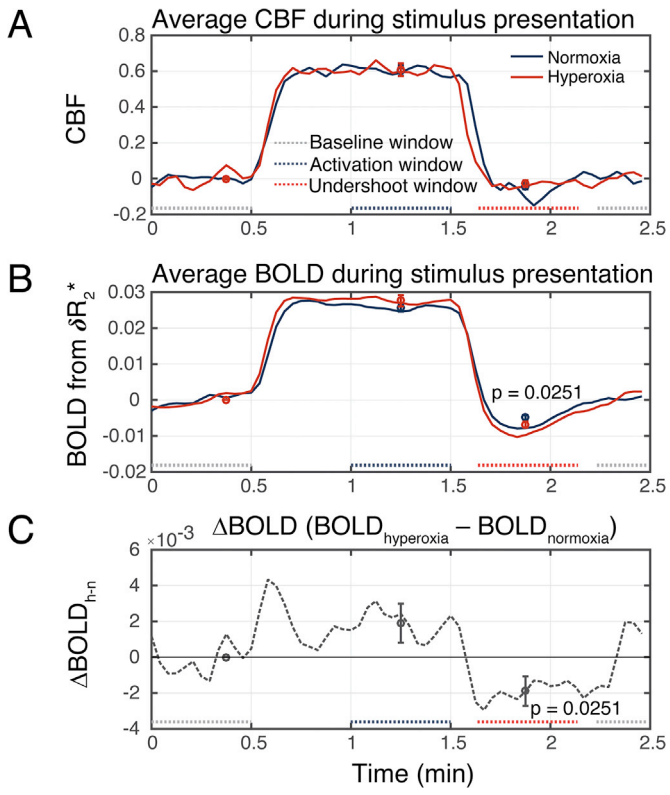

Fig. 3. CBF, BOLD, and CBV_{dHb} dynamics. (A) The CBF and (B) BOLD time courses before, during, and after visual stimulation. Curves shown here represent the average of two stimulus blocks from the two gas conditions; dotted lines above x-axes indicate time range over which measurements were averaged for the respective windows. Average values and standard errors across subjects are presented as circles and error bars on the curves and summarized in Table 1. CBF increases significantly during the visual stimulus, with no statistical difference in CBF between normoxia and hyperoxia, and a significant undershoot in normoxia CBF. BOLD increased with the visual stimulus and showed typical post-stimulus undershoot (normoxia). P-values refer to significance of difference between hyperoxia and normoxia value. (C) Difference curve represents $\Delta BOLD_{h\text{-}n} = BOLD_{hyperoxia} - BOLD_{normoxia}$ across stimulus window. P-value refers to significance of difference from zero. There was a significant difference between BOLD in hyperoxia and normoxia during the undershoot period, leading to significantly negative $\Delta BOLD_{h\text{-}n}$ and thus negative ΔCBV_{dHb}.

3.2.1. Modeling the BOLD signal

We used the classic Davis model to estimate the size of effects predicted for these experiments (Buxton, 2013; Davis et al., 1998). The BOLD signal is modeled as a function of the venous blood volume V and the magnetic susceptibility difference between the intravascular and extravascular spaces. This susceptibility difference is assumed to be zero when there is no dHb in the vessel, and to increase linearly with the venous dHb concentration C. The BOLD signal, the fractional change in signal from a baseline state (subscript "0") and an active state, is modeled as:

$$\delta b = -k\left[VC^{\beta} - V_0 C_0^{\beta}\right] \quad [1]$$

where k is a scaling factor that depends on magnetic field and echo time, and the exponent β is meant to capture the average nonlinearity of the effect of deoxyhemoglobin on the measured signal. We assume that Eq. (1) can be applied to each of the average signals during the three epochs of our experiment (baseline, primary activation, and post-stimulus

undershoot) with appropriate average values of V and C during those windows. This assumes that the post-stimulus undershoot is long enough to be treated in a quasi-static way. In normoxia, the O_2 extraction fraction E can be well-approximated by the change in O_2 bound to hemoglobin, so that $C/C_0 = E/E_0$. The first equation can then be rewritten as:

$$\delta b = M\left[1 - \frac{V}{V_0}\left(\frac{E}{E_0}\right)^{\beta}\right] \quad [2]$$

with $M = kV_0C_0^{\beta}$. For the calibrated BOLD experiment, the volume change V is assumed to be proportional to the blood flow F as (Davis et al., 1998; Grubb et al., 1974):

$$\frac{V}{V_0} = \left(\frac{F}{F_0}\right)^{\alpha} \quad [3]$$

Writing the ratio of blood flow in the active and baseline states as $f = F/F_0$, and taking r as the ratio of $CMRO_2$ in the two states, the ratio of extraction fractions is $E/E_0 = r/f$. The BOLD signal is then:

$$\delta b = M\left[1 - f^{\alpha-\beta}r^{\beta}\right] \quad [4]$$

3.2.2. Calibrated BOLD extrapolations

The hypercapnia experiment can be analyzed with Eq. (4) and the usual assumption that CO_2 inhalation increases CBF but has a negligible effect on $CMRO_2$ ($r = 1$). Applying the calibrated BOLD approach, we first tested whether the data were of sufficient quality to conclude anything definite about metabolism in the undershoot period. That is, if we assume that there is no balloon effect, so that blood volume is always coupled to blood flow, are the BOLD and CBF changes in the undershoot more consistent with the CBF/$CMRO_2$ coupling in the activation experiment or the CO_2 experiment? For the CO_2 experiment, the CBF/$CMRO_2$ coupling ratio n, defined as the ratio of fractional change in CBF to fractional change in $CMRO_2$, or $(f\text{-}1)/(r\text{-}1)$, is assumed to be infinite. From the CO_2 experimental data, M was calculated from Eq. (4) and assumed values $\alpha = 0.2$ and $\beta = 1.3$ (Chen and Pike, 2009a,b; Mark et al., 2011), yielding $M = 0.1355$; and for assumed values $\alpha = 0.2$ and $\beta = 1$ (Blockley et al., 2015; Griffeth et al., 2013), yielding $M = 0.1802$. The CBF/$CMRO_2$ coupling ratio $n = 2.25$ ($\alpha = 0.2$ and $\beta = 1.3$) and $n = 2.41$ ($\alpha = 0.2$ and $\beta = 1$) were calculated from the normoxia visual activation data. Assuming that the coupling ratios remain constant for different amplitude responses, the expected curves in the BOLD/CBF plane were extrapolated to the undershoot region with Eq. (4), shown in Fig. 2B for assumed values of $\alpha = 0.2$ and $\beta = 1$. Both curves pass through the uncertainty ellipse of the undershoot measurements, so we cannot draw any conclusions about CBF/$CMRO_2$ coupling in the undershoot period. The remainder of the modeling focused on estimates related to the tests of the Balloon Model prediction of elevated blood volume as the source of the BOLD undershoot, based on Eqs. [1–4].

3.2.3. Estimating the size of the volume change needed to explain the BOLD undershoot

Qualitatively, a negative BOLD response, as in the post-stimulus undershoot, is thought to be due to increased dHb relative to the baseline state. The "balloon" aspect of the Balloon Model is the prediction that the excess dHb is due to a slowly recovering venous blood volume while CBF and $CMRO_2$ have returned to baseline values, so that the extraction fraction E also has returned to its baseline value E_0. The fractional increase in venous blood volume, V/V_0, needed to explain the observed BOLD undershoot can be estimated from Eq. (2), once M is determined from the BOLD and CBF responses to hypercapnia using Eq. (3) with assumed values for α and β. Fig. 4A and B show the results of applying this approach to the observed data for several combinations of the assumed values of α and β. Each scenario used the average measured CBF and BOLD responses to hypercapnia and the average BOLD undershoot in normoxia as the fixed data. Note that the blood volume change during the stimulus (Activation) depends on the choice of α, but the blood volume change needed to explain the BOLD undershoot is only weakly sensitive to the choice of α and β.

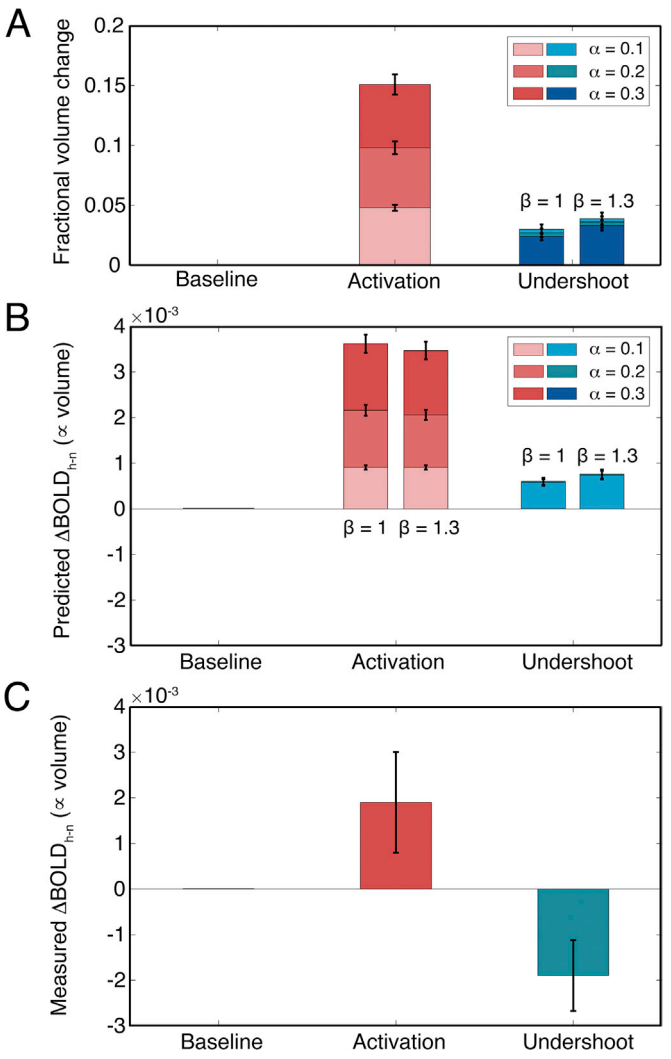

Fig. 4. Volume dynamics from experimental results compared to Balloon Model. Error bars reflect standard error across subjects. (A) Balloon Model prediction of volume dynamics needed to explain the observed BOLD undershoot as a volume effect (blue). The Davis model was used with the observed BOLD and hypercapnia data, with assumed values $\alpha = 0.1$, 0.2, 0.3, and $\beta = 1$ and $\beta = 1.3$. Activation period volume (red) calculated using observed CBF data and Grubb's power-law relationship, with assumed $\alpha = 0.1$, 0.2, 0.3. (B) Same data as A plotted in units of ΔBOLD per calculation described in section 3.2.6. (C) Experimental results from the hyperoxia and normoxia experiments, demonstrating the ΔBOLD from normoxia to hyperoxia as reflective of the volume in that state.

3.2.4. Modeling the hyperoxia effect on venous dHb

The effect of hyperoxia is to provide extra O_2 as dissolved gas in plasma that offsets the amount of O_2 removed from hemoglobin, decreasing dHb in the venous blood. An arterial blood gas measurement was not done, but we can estimate the effect of the change in pO_2 with plausible assumptions. Assuming arterial $pO_2 = 100$ mmHg with 98% arterial oxygen saturation in normoxia that increased to 100% in hyperoxia, a hemoglobin content in arterial blood of 9.3 milliequivalents of O_2 per L of blood (Davenport, 1974), and a solubility of 0.00135 mM/mmHg of dissolved O_2 in arterial blood (Valabrègue et al., 2003), the hyperoxia condition produced an average increase of about 0.43 mM in arterial O_2 concentration, or about 4.6%. For comparison,

using the same assumptions with a normoxic saturation of 98% and a typical baseline O_2 extraction fraction of 40%, the venous deoxyhemoglobin concentration in normoxia is about 3.7 mM. The added O_2 with hyperoxia then is expected to produce a decrease of venous deoxyhemoglobin concentration of about 12%.

3.2.5. Modeling the hyperoxia-BOLD effect

We assume that the effect of hyperoxia is to lower the venous dHb concentration by a small amount *w* (Blockley et al., 2013), so that $C = C_0 - w$, with *w* estimated above to be about 12% of C_0 for these experiments. For the ideal hyperoxia experiment there is no change in blood volume due to hyperoxia itself, so that $V = V_0$. Then we can apply Eq. (1) to estimate the hyperoxia-BOLD response:

$$\delta b_{O2} = kV_0\left[C_0^{\beta} - (C_0 - w)^{\beta}\right] \approx kV_0\beta w \cdot C_0^{\beta-1} \quad [5]$$

where the linear approximation applies for $w \ll C_0$. For our estimate of $w/C_0 = 0.12$, the difference in the estimate of δb_{O2} differs by only about 2% using the linear approximation compared to the full expression in Eq. (5). Note that because *k* is a physical constant, and not dependent on the particular physiological state, the hyperoxia-BOLD response depends primarily on the absolute blood volume V_0 in that state and the absolute change of venous dHb concentration *w* produced by the hyperoxia. This primary effect of blood volume on the hyperoxia-BOLD response is the motivation for the current experiments. In practice, though, this model predicts there will be an additional weak dependence on the normoxic venous dHb concentration C_0 through the second term in Eq. (5), and the potential confounding effects of this are considered below.

3.2.6. Estimating the expected hyperoxia-BOLD response

We can estimate the magnitude of the hyperoxia-BOLD response for the baseline state where we have more complete information about the state from the measurement of *M* with hypercapnia. Using the expression for *M* in the first modeling section, the hyperoxia-BOLD effect for the baseline state is:

$$\delta b_{O2}(baseline) = M\beta\frac{w}{C_0} \quad [6]$$

When interpreting this expression, it is important to remember that the value of *M* consistent with our data depends on the value of β we assume in calculating it. When β is larger, the value of *M* is smaller. As a result, the dependence of Eq. (6) on β is weaker than it at first appears to be. For our data, with $\beta = 1.0$, $\alpha = 0.2$, the product $M\beta = 0.180$, and with $\beta = 1.3$ the product $M\beta = 0.176$. Taking the $\beta = 1$ value, and assuming $w/C_0 = 0.12$ as estimated above, the estimated hyperoxia-BOLD effect for the baseline state is 0.022. Taking $\beta = 1.3$, the estimated hyperoxia-BOLD effect for the baseline state is 0.021. We then used this predicted full effect of baseline volume to predict the differences from baseline of the activation and undershoot hyperoxia-BOLD responses for the predictions of the Balloon Model. That is, the estimates of the fractional blood volume changes needed to explain the BOLD undershoot (the values plotted in Fig. 4A) were scaled with the estimated hyperoxia-BOLD effect for the baseline state to estimate what the current experiment would show. These estimates are plotted in Fig. 4B. Fig. 4C shows the mean experimentally observed differences in the hyperoxia-BOLD responses, clearly showing a qualitatively and quantitatively different pattern from the Balloon Model prediction.

3.2.7. Potential systematic errors in the hyperoxia-BOLD effect due to C_0

Our primary experimental finding is that the hyperoxia-BOLD effect is reduced in the undershoot state compared to the baseline state. By the basic interpretation of the hyperoxia-BOLD effect this is consistent with reduced venous blood volume in the undershoot period. Could this result be biased by systematic errors in the hyperoxia-BOLD response? The modeling above is based on a simple model of the BOLD effect, which in its assumptions leaves out important contributions to the BOLD signal, such as intravascular signal changes (Griffeth et al., 2013). Nevertheless, more detailed compartmental modeling of the BOLD response including these effects showed that the Davis model is reasonably accurate for describing these effects provided that *M* is measured experimentally and not estimated from first principles (Griffeth and Buxton, 2011). That is, the model expression above for *M* applies only to the extravascular signal. In general, more detailed modeling of the hyperoxia-BOLD response, as done by Blockley and colleagues (Blockley et al., 2015, 2013), is needed to better understand the systematic errors that can occur in the hyperoxia-BOLD experiment. With that caveat in mind though, the modeling above does suggest some potential errors. From Eq. (5), if $\beta > 1$, the hyperoxia-BOLD effect for a particular state will be larger for the same blood volume when the dHb concentration C_0 is larger. In our experiment, if there were no blood volume changes at all, this would translate to a response pattern opposite to what was observed (Fig. 3), with the activation hyperoxia-BOLD response smaller than that of the baseline state because of the reduced C_0, and the undershoot hyperoxia-BOLD response larger than that of the baseline state because of the increased C_0. Importantly, for testing the Balloon Model, the prediction is that venous dHb concentration is back to the baseline level during the undershoot. In that case, any difference between the baseline and undershoot hyperoxia-BOLD responses should reflect a change in the venous blood volume.

3.2.8. Potential systematic errors in the hyperoxia-BOLD effect due to reduced CBF with hyperoxia

We also found a reduction of CBF due to hyperoxia in our experiment. If this led to an overall shift of venous dHb concentration across the baseline, activation and undershoot states, we can again use Eq. (5) to estimate the systematic error produced. If the venous dHb concentration is increased by ε in each state, Eq. (5) becomes:

$$\delta b_{O2} \approx kV_0(C_0 + \varepsilon)^{\beta-1}\beta w \approx kV_0\beta w \cdot C_0^{\beta-1}\left[1 + (\beta - 1)\frac{\varepsilon}{C_0}\right] \quad [7]$$

when $\varepsilon \ll C_0$. For the limiting case of $\beta = 1$, the second term depending on C_0 goes to one, and there is no additional error due to C_0 and ε effects. Then, the hyperoxia-BOLD response for a particular state is simply proportional to the blood volume of that state. Note that for testing the Balloon Model, as in the previous section, even if $\beta > 1$, the prediction is that C_0 has returned to the baseline value, so the difference between the hyperoxia-BOLD responses in the undershoot and baseline states should still reflect the difference in the respective blood volumes. That is, by this model, the added effect of an overall change in dHb due to the CBF change should not be a confounding factor for testing the prediction of the Balloon Model. Our key experimental result is that the hyperoxia-BOLD effect is reduced in the undershoot state compared to the baseline state, opposite to the prediction of the Balloon Model and consistent with an increase of C_0 in the undershoot. Note that if ε is not the same in all states, but is instead a function of C_0, the arguments above related to testing the Balloon Model are not substantially changed. To go beyond this basic test though, and interpret the relative magnitudes of the blood volume increase with activation and the blood volume decrease in the undershoot, would require careful consideration of the additional effects of C_0 and ε described by Eq. (7).

3.2.9. The role of other vascular compartments and the meaning of "deoxygenated CBV"

In modeling the BOLD effect, the venous concentration of deoxyhemoglobin plays an important role because it is directly related to the O_2 extraction fraction, and so ties the BOLD effect to the physiological quantities CBF and $CMRO_2$, as described above. In reality, we expect that other vascular compartments also contribute to the BOLD effect depending on their volumes and dHb concentrations. A way to begin to take into account the complication of multiple vascular compartments is

to consider an effective dHb-weighted blood volume CBV_{dHb} defined such that the venous dHb concentration times this volume accurately approximates the combined effect on the BOLD signal of each compartment in the tissue:

$$CBV_{dHb}[dHb]_V \approx V_A[dHb]_A + \phi V_C[dHb]_C + V_V[dHb]_V \quad [8]$$

where A, V and C as subscripts refer to the arterial, venous and capillary compartments, and V and [dHb] as variables refer to the volume and mean deoxyhemoglobin concentration within those compartments. This approximate form retains the central role of the venous dHb concentration, and its connection to CBF and $CMRO_2$, while expanding the idea of the blood volume to include the effects of other compartments. In this equation we have included an additional parameter ϕ to model the fact that a given total dHb in capillaries has less of an effect on the BOLD signal than the same total amount of dHb in larger vessels because of motional narrowing due to diffusion around the smallest vessels (Buxton, 2013). This limits the contribution of capillaries, effectively equivalent to a lower capillary volume than the anatomical capillary volume. In the hyperoxia experiment, the dHb concentration in each compartment will go down, and the resulting hyperoxia-BOLD effect will have contributions from each of the vascular compartments, again with the capillary contribution downgraded by ϕ. In this way, the hyperoxia-BOLD effect is expected to sample all the vascular compartments that contain dHb in the normoxic state, although the precise contribution of each compartment will depend on exactly how much the dHb concentration is changed in each compartment. In short, although our earlier modeling considered only the venous compartment, these arguments suggest that the hyperoxia-BOLD experiment is also sensitive to dHb in other blood compartments as well, so that the measured blood volume likely reflects more of CBV_{dHb} than just venous blood volume.

4. Discussion

This study helps to establish a foundation for estimating the dynamics of oxygen metabolism ($CMRO_2$) in the human brain based on measuring the dynamics of blood flow (CBF) and the BOLD response. In principle, this is possible if the dynamics of the deoxygenated blood volume (CBV_{dHb}) are assumed to closely follow the dynamics of CBF. If not, the unknown dynamics of CBV_{dHb} will always be a major confounding effect for isolating the dynamics of $CMRO_2$. The BOLD post-stimulus undershoot is a prime example where significant uncoupling of CBV_{dHb} and CBF has been hypothesized. The Balloon Model (Buxton et al., 1998) and the delayed compliance Windkessel model (Mandeville et al., 1999) predict that this phenomenon is due to elevated venous CBV in the presence of normalized or reduced CBF (Buxton et al., 1998). For this reason, we took the post-stimulus undershoot as an important test case; specifically, is CBV_{dHb} elevated during the undershoot? While there are several methods for measuring total CBV, isolating the deoxyhemglobin-weighted fraction is more challenging. Previous modeling studies (Blockley et al., 2013) found that the hyperoxia-BOLD response, the change between normoxia and hyperoxia in a particular state, is proportional to CBV_{dHb} in that state. We measured the activation and undershoot responses to a visual stimulus in both normoxia and hyperoxia, then compared the hyperoxia-BOLD response in the undershoot to that in the baseline state. The Balloon Model predicts that this response should be larger in the undershoot period, but our experimental finding showed that it is significantly smaller, arguing against a slowly recovering blood volume during the undershoot.

To further inform the interpretation of this result, we used a model of the BOLD effect to predict the magnitude of the blood volume change that would be required to explain the BOLD undershoot, and then to estimate how that blood volume change would translate to the hyperoxia-BOLD effect measured here. The modeling was also used to consider potential systematic errors involved in interpreting the hyperoxia-BOLD effect as a pure reflection of blood volume. For example, in our experiment we found that hyperoxia administration reduced CBF, and our concern was whether this additional effect would confound our test of the Balloon Model. The modeling suggests that the hyperoxia experiment is relatively robust for testing the prediction of the Balloon Model, because that prediction primarily depends on whether the hyperoxia-BOLD response in the undershoot is greater than or less than the hyperoxia-BOLD response in the baseline state. However, extending the interpretation to quantitative estimates of the volume changes in different states would require more extensive modeling of the experiment.

4.1. Origin of the BOLD post-stimulus undershoot

Our findings show no evidence of elevated CBV during the post-stimulus undershoot and are consistent with previous studies using techniques sensitive to *total* CBV in humans (Frahm et al., 2008; Lu et al., 2004; van Zijl et al., 2012). Our data also are consistent with a study using a different method, venous refocusing for volume estimation (VERVE) (Stefanovic and Pike, 2005), specifically focused on venous CBV changes in humans. In the latter study, there was evidence for increased venous CBV during a visual stimulus, but no evidence for increased venous CBV during the post-stimulus period.

If slow CBV recovery is not the dominant cause of the post-stimulus undershoot, it is likely to be due to some combination of reduced CBF and a slow recovery of $CMRO_2$. In most studies, the interpretation of the two possibilities hinges on whether there is a detectable undershoot of CBF. If not, elevated $CMRO_2$ is implicated (Frahm et al., 2008; Hua et al., 2011; Lu et al., 2004; van Zijl et al., 2012). Our experimental results indicate that blood volume is decreased during the undershoot, which would be consistent with a CBF decrease and coupled blood flow and blood volume. We also found a modest but statistically significant undershoot of CBF in normoxia, but not during hyperoxia. The difference between these two undershoot signals was not statistically significant. In addition, our modeling results suggest that we should be cautious about interpreting the relative magnitudes of the hyperoxia-BOLD effect between states as a pure reflection of blood volume when the venous oxygenation varies between the states, as would be the case during the BOLD undershoot if CBF is reduced or $CMRO_2$ is elevated. For these reasons, we cannot conclude anything about the quantitative coupling of blood flow and blood volume during the undershoot, except to note that the data are consistent with a reduction of both. Previous human studies have found statistically significant undershoots of CBF during the BOLD undershoot (Chen and Pike, 2009a,b; Griffeth and Buxton, 2011). Recent work by Mullinger et al. (2017) using simultaneously recorded EEG, BOLD, and CBF responses to visual stimuli provided evidence for a CBF undershoot with a decrease in the $CBF/CMRO_2$ coupling ratio in the post-stimulus phase compared with the primary stimulus phase.

4.2. Blood volume dynamics

Beyond the phenomenon of the post-stimulus undershoot, the more general question is whether a venous component of CBV changes more slowly than CBF. Two animal model studies, based on anatomical measurements of venous vessels (Drew et al., 2011) and magnetization transfer (MT)-varied BOLD and contrast-agent fMRI techniques (Kim and Kim, 2011), found evidence for a slow expansion and recovery of venous CBV with a time constant on the order of 40 s, so that this effect was only observable with long stimuli. This was consistent with other anatomical studies, which found no change in venous CBV for shorter stimuli (Devor et al., 2007; Hillman et al., 2007). In a recent study in humans, our group looked at continuously varying stimuli with periods ranging from 6.3 s to 44 s over long time periods (~5 min), measuring the dynamics of BOLD and CBF (Simon and Buxton, 2015). Venous CBV was not measured, but the consistency of coupling of CBF and BOLD across stimuli could be used to test for the presence of a slow component, which could be due to either venous CBV or $CMRO_2$. Interestingly, across different oscillation periods,

the coupling was consistent (no evidence of a slow component), but across the full 5 min of the run there was evidence of a component an order of magnitude slower to develop than CBF. Taken together, these studies suggest that there is a slow component of CBV change that only becomes important with very long stimuli. In our current study, the SNR was not sufficient to detect the effects of such a slow CBV_{dHb} change during the 1-min stimulation.

4.3. Limitations of the current study

This study has several limitations, a primary one being that the signal changes involved in estimating CBV_{dHb} changes are quite small, so comparing exact magnitudes of change is likely to be unreliable with these data. Nevertheless, this is a method that is specifically sensitive to deoxygenated CBV, and the sign of the measured changes argues against the undershoot being primarily due to elevated venous CBV. The original theoretical treatments of the effects of hyperoxia focused on changes due to hyperoxia when the underlying physiology remained constant (Blockley et al., 2013). Here we have extended that idea to looking at each segment of a dynamic response as a sequence of physiological steady-states. While this is plausible for the long positive response during the stimulus, it is not as clear that this is justified for the undershoot period. More detailed modeling is needed to address this assumption. In addition, hyperoxia itself can alter both the physical and physiological state. The act of breathing elevated O_2 can subtly alter magnetic field gradients with an uncertain effect on the MR signal. More importantly, hyperoxia can alter the physiological state. In our study, we found a reduction of CBF due to hyperoxia. Potentially, the use of additional control hardware for gas delivery that clamps arterial pO_2 and pCO_2 values could have prevented the CBF change. We assumed that these additional effects of hyperoxia created an unknown artifactual offset of δR_2* in moving from the normoxic to the hyperoxic condition, and that this was the same across the baseline, activation and undershoot states. Our modeling, however, indicates that this effect could vary depending on the venous deoxyhemoglobin concentration. Importantly, though, this is not a confounding effect for the basic test of the Balloon Model, because the prediction is that venous deoxyhemoglobin concentration has returned to the baseline value. In short, the hyperoxia method remains a relatively robust test of the Balloon Model, but we should be cautious in interpreting the magnitude of the blood volume changes between states from these data. More detailed modeling may enable additional interpretation of these data.

5. Conclusions

We found no evidence of a slower recovery of blood volume during the BOLD post-stimulus undershoot period, contrary to the prediction of the Balloon Model. Taken together with a wide range of studies in humans and animal models, the emerging picture is that slow changes in venous blood volume occur only for extended duration stimuli. This has important implications for estimating the dynamics of oxygen metabolism from dynamic CBF and BOLD measurements, and provides support for two key assumptions: 1) for stimuli of modest duration (<1-min), the slow component of blood volume change can be neglected, and 2) the faster blood volume changes track with the CBF change. While more work is needed to fully justify these assumptions, this emerging view opens the door for measurements of the dynamics of oxygen metabolism in the human brain that are not possible with any other method.

Funding sources

This work was supported by the National Institutes of Health NS036722, NS085478, MH111359, and MH113295.

Acknowledgements

The authors acknowledge Kenny Jackson, Abel Martinez, and Jessica Ho for their help in data acquisition; David Shin, Kun Lu, and Aaron Simon for their advice and expertise with various imaging sequences and analyses; and Interfaces Graduate Training Program and the UCSD Medical Scientist Training Program for support and funding.

References

Blockley, N.P., Griffeth, V.E.M., Buxton, R.B., 2012. A general analysis of calibrated BOLD methodology for measuring CMRO 2 responses: comparison of a new approach with existing methods. Neuroimage 60, 279–289. https://doi.org/10.1016/j.neuroimage.2011.11.081.

Blockley, N.P., Griffeth, V.E.M., Germuska, M. a., Bulte, D.P., Buxton, R.B., 2013. An analysis of the use of hyperoxia for measuring venous cerebral blood volume: comparison of the existing method with a new analysis approach. Neuroimage 72, 33–40. https://doi.org/10.1016/j.neuroimage.2013.01.039.

Blockley, N.P., Griffeth, V.E.M., Stone, A.J., Hare, H.V., Bulte, D.P., 2015. Sources of systematic error in calibrated BOLD based mapping of baseline oxygen extraction fraction. Neuroimage 122, 105–113. https://doi.org/10.1016/j.neuroimage.2015.07.059.

Boynton, G.M., Engel, S.A., Glover, G.H., Heeger, D.J., 1996. Linear systems analysis of functional magnetic resonance imaging in human V1. J. Neurosci. 16, 4207–4221.

Brainard, D.H., 1997. The psychophysics Toolbox. Spat. Vis. 10, 433–436. https://doi.org/10.1163/156856897X00357.

Bulte, D.P., Chiarelli, P. a, Wise, R.G., Jezzard, P., 2007. Cerebral perfusion response to hyperoxia. J. Cereb. Blood Flow Metab. 27, 69–75. https://doi.org/10.1038/sj.jcbfm.9600319.

Buxton, R.B., 2013. The physics of functional magnetic resonance imaging (fMRI). Rep. Prog. Phys. 76, 96601. https://doi.org/10.1088/0034-4885/76/9/096601.

Buxton, R.B., Wong, E.C., Frank, L.R., 1998. Dynamics of blood flow and oxygenation changes during brain activation: the balloon model. Magn. Reson. Med. 39, 855–864. https://doi.org/10.1002/mrm.1910390602.

Chalela, J. a, Alsop, D.C., Gonzalez-Atavales, J.B., Maldjian, J. a, Kasner, S.E., Detre, J. a, 2000. Magnetic resonance perfusion imaging in acute ischemic stroke using continuous arterial spin labeling. Stroke 31, 680–687. https://doi.org/10.1161/01.STR.31.3.680.

Chen, J.J., Pike, G.B., 2009a. Origins of the BOLD post-stimulus undershoot. Neuroimage 46, 559–568. https://doi.org/10.1016/j.neuroimage.2009.03.015.

Chen, J.J., Pike, G.B., 2009b. BOLD-specific cerebral blood volume and blood flow changes during neuronal activation in humans. NMR Biomed. 22, 1054–1062. https://doi.org/10.1002/nbm.1411.

Cox, R.W., 1996. AFNI: software for analysis and visualization of functional magnetic resonance neuroimages. Comput. Biomed. Res. 29, 162–173. https://doi.org/10.1006/cbmr.1996.0014.

Davenport, H.W., 1974. The ABC of Acid-base Chemistry, Sixth. ed. The University of Chicago Press, Chicago, IL.

Davis, T.L., Kwong, K.K., Weisskoff, R.M., Rosen, B.R., 1998. Calibrated functional MRI: mapping the dynamics of oxidative metabolism. Proc. Natl. Acad. Sci. U. S. A. 95, 1834–1839. https://doi.org/10.1073/pnas.95.4.1834.

Devor, A., Tian, P., Nishimura, N., Teng, I.C., Hillman, E.M.C., Narayanan, S.N., Ulbert, I., Boas, D.A., Kleinfeld, D., Dale, A.M., 2007. Suppressed neuronal activity and concurrent arteriolar vasoconstriction may explain negative blood oxygenation level-dependent signal. J. Neurosci. 27, 4452–4459. https://doi.org/10.1523/JNEUROSCI.0134-07.2007.

Drew, P.J., Shih, A.Y., Kleinfeld, D., 2011. Fluctuating and sensory-induced vasodynamics in rodent cortex extend arteriole capacity. Proc. Natl. Acad. Sci. U. S. A. 108, 8473–8478. https://doi.org/10.1073/pnas.1100428108.

Frahm, J., Baudewig, J., Kallenberg, K., Kastrup, A., Merboldt, K.D., Dechent, P., 2008. The post-stimulation undershoot in BOLD fMRI of human brain is not caused by elevated cerebral blood volume. Neuroimage 40, 473–481. https://doi.org/10.1016/j.neuroimage.2007.12.005.

Griffeth, V.E.M., Blockley, N., Simon, A.B., Buxton, R.B., 2013. A new functional MRI approach for investigating modulations of brain oxygen metabolism. PLoS One 8, e68122. https://doi.org/10.1371/journal.pone.0068122.

Griffeth, V.E.M., Buxton, R.B., 2011. A theoretical framework for estimating cerebral oxygen metabolism changes using the calibrated-BOLD method: modeling the effects of blood volume distribution, hematocrit, oxygen extraction fraction, and tissue signal properties on the BOLD signal. Neuroimage 58, 198–212. https://doi.org/10.1016/j.neuroimage.2011.05.077.

Grubb, R.L., Raichle, M.E., Eichling, J.O., Ter-Pogossian, M.M., 1974. The effects of changes in PaCO2 on cerebral blood volume, blood flow, and vascular mean transit time. Stroke 5, 630–639. https://doi.org/10.1161/01.STR.5.5.630.

Hillman, E.M.C., Devor, A., Bouchard, M.B., Dunn, A.K., Krauss, G.W., Skoch, J., Bacskai, B.J., Dale, A.M., Boas, D. a., 2007. Depth-resolved optical imaging and microscopy of vascular compartment dynamics during somatosensory stimulation. Neuroimage 35, 89–104. https://doi.org/10.1016/j.neuroimage.2006.11.032.

Hua, J., Stevens, R.D., Huang, A.J., Pekar, J.J., van Zijl, P.C.M., 2011. Physiological origin for the BOLD poststimulus undershoot in human brain: vascular compliance versus oxygen metabolism. J. Cereb. Blood Flow Metab. 31, 1599–1611. https://doi.org/10.1038/jcbfm.2011.35.

Kim, T., Kim, S.-G., 2011. Temporal dynamics and spatial specificity of arterial and venous blood volume changes during visual stimulation: implication for bold quantification. J. Cereb. Blood Flow Metab. 31, 1211–1222. https://doi.org/10.1038/jcbfm.2010.226.

Kirchner, W.K., 1958. Age differences in short-term retention of rapidly changing information. J. Exp. Psychol. 55, 352–358. https://doi.org/10.1037/h0043688.

Kwong, K.K., Belliveau, J.W., Chesler, D.A., Goldberg, I.E., Weisskoff, R.M., Poncelet, B.P., Kennedy, D.N., Hoppel, B.E., Cohen, M.S., Turner, R., 1992. Dynamic magnetic resonance imaging of human brain activity during primary sensory stimulation. Proc. Natl. Acad. Sci. U. S. A. 89, 5675–5679. https://doi.org/10.1073/pnas.89.12.5675.

Liu, T.T., Behzadi, Y., Restom, K., Uludag, K., Lu, K., Buracas, G.T., Dubowitz, D.J., Buxton, R.B., 2004. Caffeine alters the temporal dynamics of the visual BOLD response. Neuroimage 23, 1402–1413. https://doi.org/10.1016/j.neuroimage.2004.07.061.

Liu, T.T., Wong, E.C., 2005. A signal processing model for arterial spin labeling functional MRI. Neuroimage 24, 207–215. https://doi.org/10.1016/j.neuroimage.2004.09.047.

Lu, H., Golay, X., Pekar, J.J., Van Zijl, P.C.M., 2004. Sustained poststimulus elevation in cerebral oxygen utilization after vascular recovery. J. Cereb. Blood Flow Metab. 24, 764–770. https://doi.org/10.1097/01.WCB.0000124322.60992.5C.

Mandeville, J.B., Marota, J.J., Ayata, C., Zaharchuk, G., Moskowitz, M. a, Rosen, B.R., Weisskoff, R.M., 1999. Evidence of a cerebrovascular postarteriole windkessel with delayed compliance. J. Cereb. Blood Flow Metab. 19, 679–689. https://doi.org/10.1097/00004647-199906000-00012.

Mandeville, J.B., Marota, J.J., Kosofsky, B.E., Keltner, J.R., Weissleder, R., Rosen, B.R., Weisskoff, R.M., 1998. Dynamic functional imaging of relative cerebral blood volume during rat forepaw stimulation. Magn. Reson. Med. 39, 615–624. https://doi.org/10.1002/mrm.1910390415.

Mark, C.I., Fisher, J.A., Pike, G.B., 2011. Improved fMRI calibration: precisely controlled hyperoxic versus hypercapnic stimuli. Neuroimage 54, 1102–1111. https://doi.org/10.1016/j.neuroimage.2010.08.070.

Mullinger, K.J., Cherukara, M.T., Buxton, R.B., Francis, S.T., Mayhew, S.D., 2017. Post-stimulus fMRI and EEG responses: Evidence for a neuronal origin hypothesised to be inhibitory. Neuroimage 157, 388–399. https://doi.org/10.1016/j.neuroimage.2017.06.020.

Noll, D.C., Fessler, J.A., Sutton, B.P., 2005. Conjugate phase MRI reconstruction with spatially variant sample density correction. IEEE Trans. Med. Imag. 24, 325–336. https://doi.org/10.1109/TMI.2004.842452.

Pelli, D.G., 1997. The VideoToolbox software for visual psychophysics: transforming numbers into movies. Spat. Vis. 10, 437–442. https://doi.org/10.1163/156856897X00366.

Perthen, J.E., Lansing, A.E., Liau, J., Liu, T.T., Buxton, R.B., 2008. Caffeine-induced uncoupling of cerebral blood flow and oxygen metabolism: a calibrated BOLD fMRI study. Neuroimage 40, 237–247. https://doi.org/10.1016/j.neuroimage.2007.10.049.

Pike, G.B., 2012. Quantitative functional MRI: concepts, issues and future challenges. Neuroimage. https://doi.org/10.1016/j.neuroimage.2011.10.046.

Pilkinton, D.T., Gaddam, S.R., Reddy, R., 2011. Characterization of paramagnetic effects of molecular oxygen on blood oxygenation level-dependent-modulated hyperoxic contrast studies of the human brain. Magn. Reson. Med. 66, 794–801. https://doi.org/10.1002/mrm.22870.

Simon, A.B., Buxton, R.B., 2015. Understanding the dynamic relationship between cerebral blood flow and the BOLD signal: implications for quantitative functional MRI. Neuroimage 116, 158–167. https://doi.org/10.1016/j.neuroimage.2015.03.080.

Simon, A.B., Dubowitz, D.J., Blockley, N.P., Buxton, R.B., 2016. A novel Bayesian approach to accounting for uncertainty in fMRI-derived estimates of cerebral oxygen metabolism fluctuations. Neuroimage 129, 198–213. https://doi.org/10.1016/j.neuroimage.2016.01.001.

Stefanovic, B., Pike, G.B., 2005. Venous refocusing for volume estimation: VERVE functional magnetic resonance imaging. Magn. Reson. Med. 53, 339–347. https://doi.org/10.1002/mrm.20352.

Valabrègue, R., Aubert, A., Burger, J., Bittoun, J., Costalat, R., 2003. Relation between cerebral blood flow and metabolism explained by a model of oxygen exchange. J. Cereb. Blood Flow Metab. 23, 536–545. https://doi.org/10.1097/01.WCB.0000055178.31872.38.

van Zijl, P.C.M., Hua, J., Lu, H., 2012. The BOLD post-stimulus undershoot, one of the most debated issues in fMRI. Neuroimage 62, 1092–1102. https://doi.org/10.1016/j.neuroimage.2012.01.029.

Wang, J., Qiu, M., Constable, R.T., 2005. In vivo method for correcting transmit/receive nonuniformities with phased array coils. Magn. Reson. Med. 53, 666–674. https://doi.org/10.1002/mrm.20377.

Wong, E.C., Buxton, R.B., Frank, L.R., 1998. Quantitative imaging of perfusion using a single subtraction (QUIPSS and QUIPSS II). Magn. Reson. Med. 39, 702–708. https://doi.org/10.1002/mrm.1910390506.